

Supporting Information

Interface Coassembly of Mesoporous MoS₂ Based-Frameworks for Enhanced Near-Infrared Light Driven Photocatalysis

Lihua Zhi,^a Haoli Zhang,^a Zhengyin Yang,^a Weisheng Liu,^a and Baodui Wang^{*a}

1. Materials. iron(III) acetylacetonate (99.9%), copper(II) acetylacetonate (99.9%), oleylamine, α -thioctic acid (LA), dopamine hydrochloride (DPA) and N-Ethoxycarbonyl-2-ethoxy-1,2-dihydroquinoline (EEDQ), were purchased from Sigma-Aldrich. Molybdenum (IV) sulfide (MoS₂, 99%) was purchased from Alfa Aesar. 1.6 M n-butyllithium solution, graphite powder were purchased from J&K Scientific Ltd. (China). All chemicals were used without further purification. MoS₂ nanosheet solution was synthesized by chemical exfoliation method using similar method according to the literature.¹ Fe₃O₄@Cu_{2-x}S NPs,² Fe₃O₄ NPs³ and CuFe₂O₄ NPs⁴ were prepared according to the literature.

2. Measurements. ¹H NMR spectra and ¹³C NMR spectra were acquired with Varian 400 MHz NMR. Magnetic properties were recorded on a Lakeshore 7404 high-sensitivity vibrating sample magnetometer (VSM) with fields up to 1.5 tesla at room temperature. The morphology of the samples was investigated by field-emission scanning electron microscope (FE-SEM, FEI, Sirion 200). TEM images were taken on Tecna i-G2-F30 (FEI) transmission electron microscope at an acceleration voltage of 300 kV. X-ray powder diffraction (XRD) patterns of the nanomaterials were recorded on a Bruker AXS D8-Advanced diffractometer with Cu K α radiation ($\lambda=1.5418\text{\AA}$). N₂ adsorption-desorption isotherms were measured at 77 K after heating the samples at 100 °C for 8 h to remove any moisture and solvent molecules presented in the pores with Micromeritics TriStar II 3020 analyzer. The Brunauer-Emmett-Teller (BET) method was utilized to calculate the specific surface areas (S_{BET}). By using the Barrett-Joyner-Halenda (BJH) model, the pore volumes and pore size distributions were derived from the adsorption branches of isotherms. X-ray photoelectron spectroscopy (XPS) measurements were performed on a PHI-5702 multifunctional spectrometer using AlK α radiation. Raman spectra were collected using a confocal microprobe Raman system (Renishaw, RM2000). FT-IR spectra were recorded on a Nicolet FT-170SX spectrometer. Au and Fe contents are determined by inductively coupled plasma-atomic emission

spectrometry (ICP-AES, Varian VISTA-MPX). UV-vis-NIR absorption spectra were carried out on a Agilent Cary 5000 UV-Vis-NIR Spectrophotometer. Photocatalysis was performed using Xenon lamp (HSX-F300), equipped with 700 nm cutoff filter. The yields were determined by 450-GC gas chromatograph.

3. Experimental section

3.1. Synthesis of N-(3,4-dihydroxyphenethyl)-5-(1,2-dithiolan-3-yl) pentanamide (LA-DPA).

Triethylamine (0.1012 g) was added drop-wise to 20 mL ethanol under nitrogen, which containing 0.1896 g dopamine hydrochloride (DPA). The mixture was stirred at room temperature for 1h. Then, α -thioctic acid 0.2064 g (1 mmol) and EEDQ 0.2473 g (1 mmol) were added to the solution. After stirring for 24 h at room temperature under nitrogen atmosphere, the insoluble product was filtered, and the filtrate was evaporated. The residue was purified by column chromatography on silica gel to give LA-DPA as yellow oily liquid. (0.2425 g, yield, 71%). ESI-MS: $m/z = 342.1721$ for $[M+H]^+$. IR (KBr plate, cm^{-1}): 3351 (s), 2924 (s), 2860 (m), 2721 (w), 2570 (w), 1754 (m), 1707 (m), 1636 (s), 1522 (s), 1442 (s), 1367 (s), 1282 (s), 1253 (s), 1197 (s), 1115 (m), 1048 (m), 955 (w), 874 (w), 812 (m), 784 (m), 633 (m), 589 (m), 450 (w). ^1H NMR (400MHz, CDCl_3), δ (ppm): 8.73 (s, 2H), 7.85-7.82 (t, 1H), 6.65-6.63 (d, 1H), 6.59 (s, 1H), 6.46-6.42 (dd, 1H), 3.62-3.50 (m, 2H), 3.21-3.07 (m, 4H), 2.44-2.36 (m, 1H), 2.07-2.04 (t, 2H), 1.89-1.81 (m, 1H), 1.67-1.60 (m, 1H), 1.56-1.47 (m, 3H), 1.36-1.28 (m, 2H).

3.2. Synthesis of DPA-MoS₂. 10 mg of LA-DPA was dissolved in 10 mL DMF and then mixed with 20 mL MoS₂NSs (2 mg/mL) aqueous dispersion. After the mixture sonicated for 1h and stirred overnight, the formed DPA-MoS₂ was collected by centrifuging and washed thoroughly several times with DMF and water. IR (KBr plate, cm^{-1}): 3431 (m), 1626 (m), 1572 (w), 1344 (m), 1240 (m), 1142 (s), 1044 (s), 1013 (s), 874 (s), 668 (s), 591 (s).

3.3 Preparation of 3D Fe₃O₄@Cu_{2-x}S-MoS₂F. 20 mg of DPA-MoS₂ was dissolved in 30 mL DMF and 20 mL DCM to form a homogeneous solution. After sonication for 30 min, Fe₃O₄@Cu_{2-x}S (5 mg) in 10 mL DCM was added drop-wise to the above solution. The mixture was sonicated for 1h, and then stirred overnight at room temperature. After the reaction finished, 3D Fe₃O₄@Cu_{2-x}S-MoS₂F was collected by centrifuging and washed thoroughly several times with CH₂Cl₂. IR (KBr plate, cm^{-1}): 3427 (m), 1697 (w), 1629 (s), 1551 (w), 1415 (m), 1357 (w), 1090 (s), 906 (s), 730 (m), 656 (w), 596 (w), 553 (s), 459 (m).

3.4 Synthesis of aryldiazonium salts. The aryldiazonium salts were prepared according to the literature with slight modification.⁵ The corresponding aniline (0.02 mol) was dissolved in a mixture of ultrapure water (8 mL) and 50% fluoroboric acid (7 mL). After the temperature fell below zero, 3 mL sodium nitrite solution (1.38 g) was added slowly. The mixture was stirred for 30 minutes in ice bath, and the resulting precipitate was collected by centrifuging and washed several times with CH₂Cl₂. The resulting solid was recrystallized by acetone and CH₂Cl₂.

3.5 General procedure for the 3D Fe₃O₄@Cu_{2-x}S-MoS₂F catalyzed arylation of furan. aryldiazonium tetrafluoroborate (0.1 mmol), 3D Fe₃O₄@Cu_{2-x}S-MoS₂F (2 mg), 1 mL EtOH and 1 mL furan were added to a 10 mL glass tube. Then, the glass tube was closed, evacuated and refilled with nitrogen (N₂). The resulting mixture was stirred under irradiation (distance 10 cm) for 1h. After reaction finished, the catalysts were collected by centrifuging and the centrifugal liquid was evaporated. The residue was purified by flash chromatography and isolated.

3.6 General procedure for the 3D Fe₃O₄@Cu_{2-x}S-MoS₂F catalyzed arylation of thiophene. aryldiazonium tetrafluoroborate (0.1 mmol), 3D Fe₃O₄@Cu_{2-x}S-MoS₂F (2 mg), 1 mL EtOH and 1 mL thiophene were added to a 10 mL glass tube. Then, the glass tube was closed, evacuated and refilled with nitrogen (N₂). The resulting mixture was stirred under irradiation (distance 10 cm) for 1h. After reaction finished, the catalysts were collected by centrifuging and the centrifugal liquid was evaporated. The residue was purified by flash chromatography and isolated.

3.7 General procedure for the 3D Fe₃O₄@Cu_{2-x}S-MoS₂F catalyzed arylation of pyridine. aryldiazonium tetrafluoroborate (0.1 mmol), 3D Fe₃O₄@Cu_{2-x}S-MoS₂F (2 mg), 1 mL CH₃COCH₃ and 1 mL pyridine were added to a 10 mL glass tube. Then, the glass tube was closed, evacuated and refilled with nitrogen (N₂). The resulting mixture was stirred under irradiation (distance 10 cm) for 1h. After reaction finished, the catalysts were collected by an external magnetic field and the liquid was evaporated. The residue was purified by flash chromatography and isolated.

3.8 General procedure for 3D Fe₃O₄@Cu_{2-x}S-MoS₂F recycling. aryldiazonium tetrafluoroborate (0.1 mmol), 3D Fe₃O₄@Cu_{2-x}S-MoS₂F (2 mg), 1 mL CH₃COCH₃ and 1 mL furan were added to a 10 mL glass tube. Then, the glass tube was closed, evacuated and refilled with nitrogen (N₂). The resulting mixture was stirred under irradiation (distance 10 cm) for 1h. After reaction finished, the mixture was treated with an external magnetic field and the resulting liquid was taken off. Then the fresh reactants were added again to start the next round of reaction.

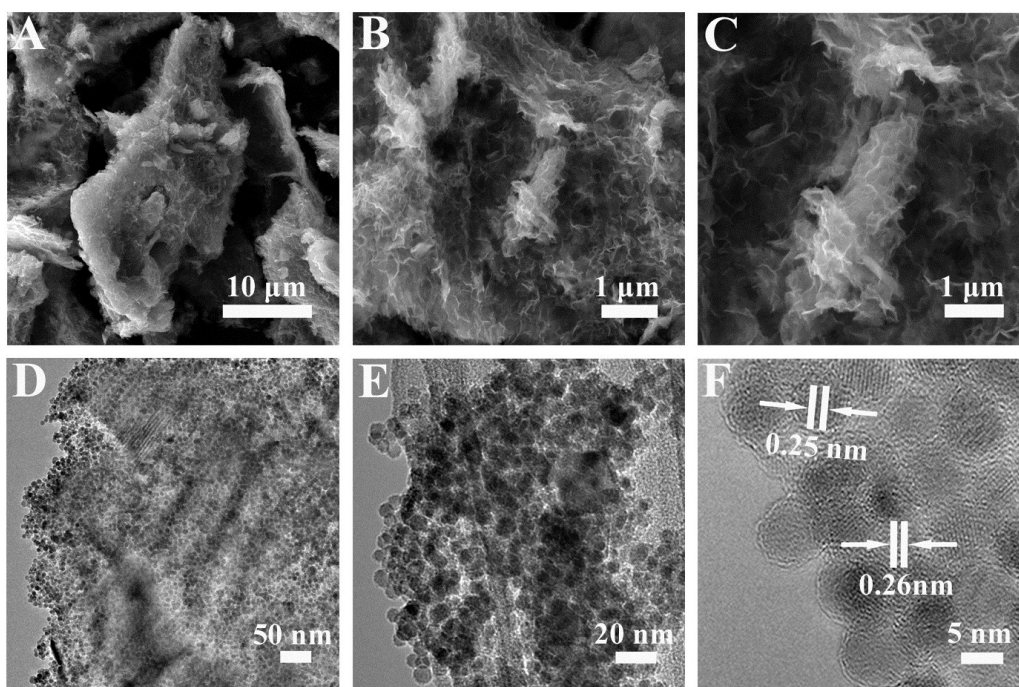


Figure S1. Different magnification SEM images (A-C) and TEM images (D-E) of the 3D $\text{Fe}_3\text{O}_4\text{-MoS}_2\text{F}$. (F) HRTEM image of the 3D $\text{Fe}_3\text{O}_4\text{-MoS}_2\text{F}$.

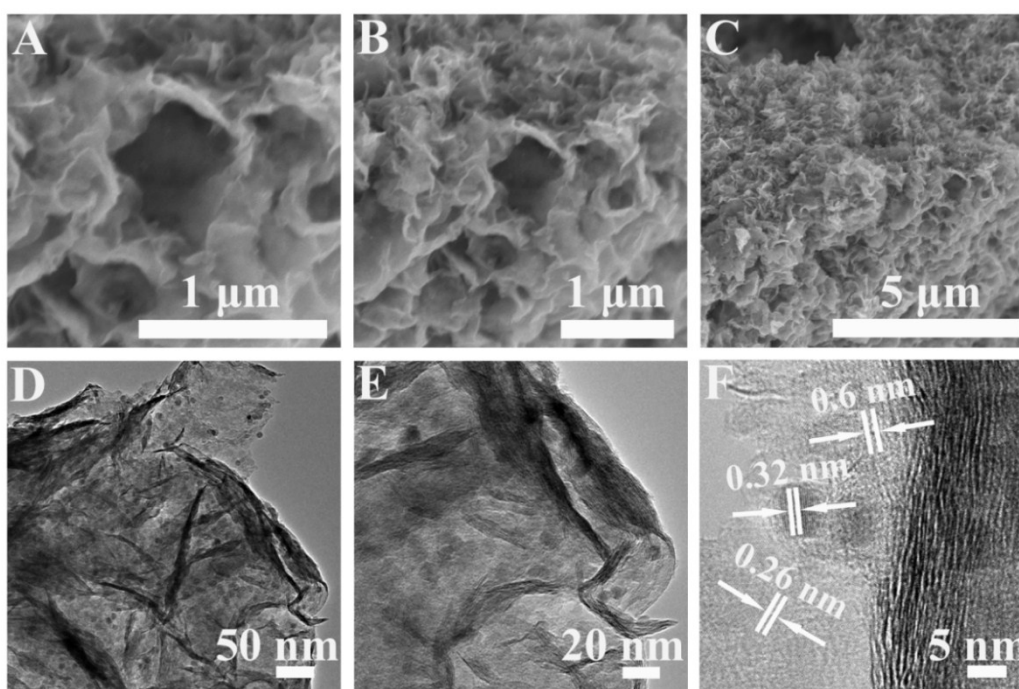


Figure S2 Different magnification SEM images (A-C) and TEM images (D-E) of the 3D $\text{CuFe}_2\text{O}_4\text{-MoS}_2\text{F}$. (F) HRTEM image of the 3D $\text{CuFe}_2\text{O}_4\text{-MoS}_2\text{F}$.

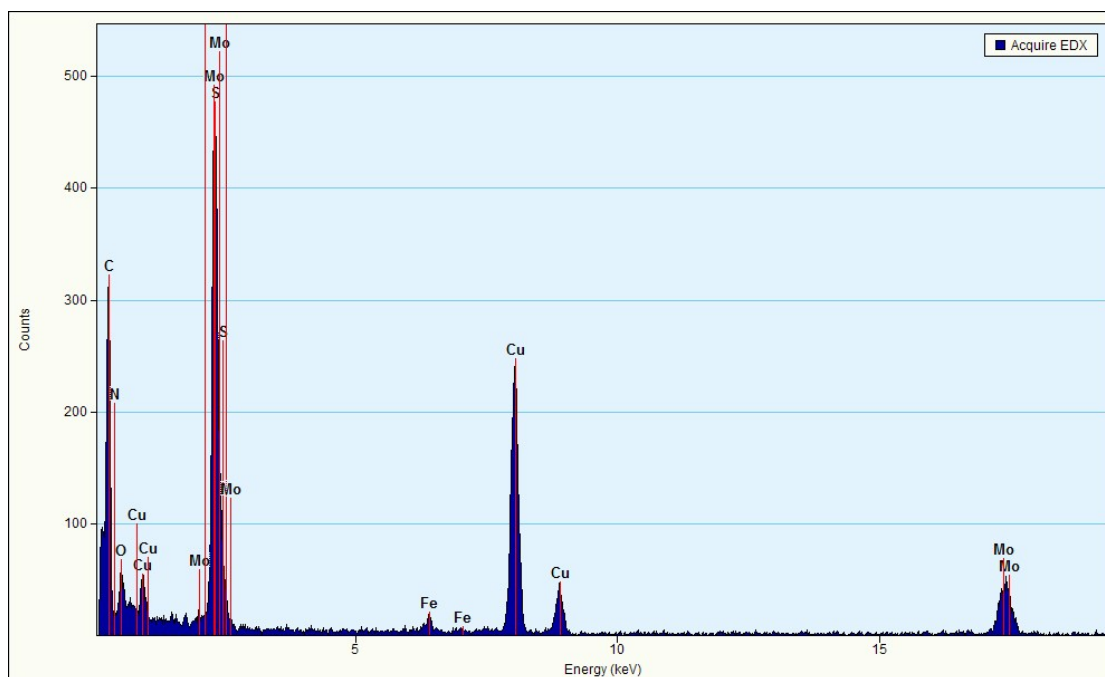


Figure S3. EDX data of the 3D $\text{Fe}_3\text{O}_4@Cu_{2-x}\text{S-MoS}_2\text{F}$. Note that the peaks of Mo and S are overlapped.

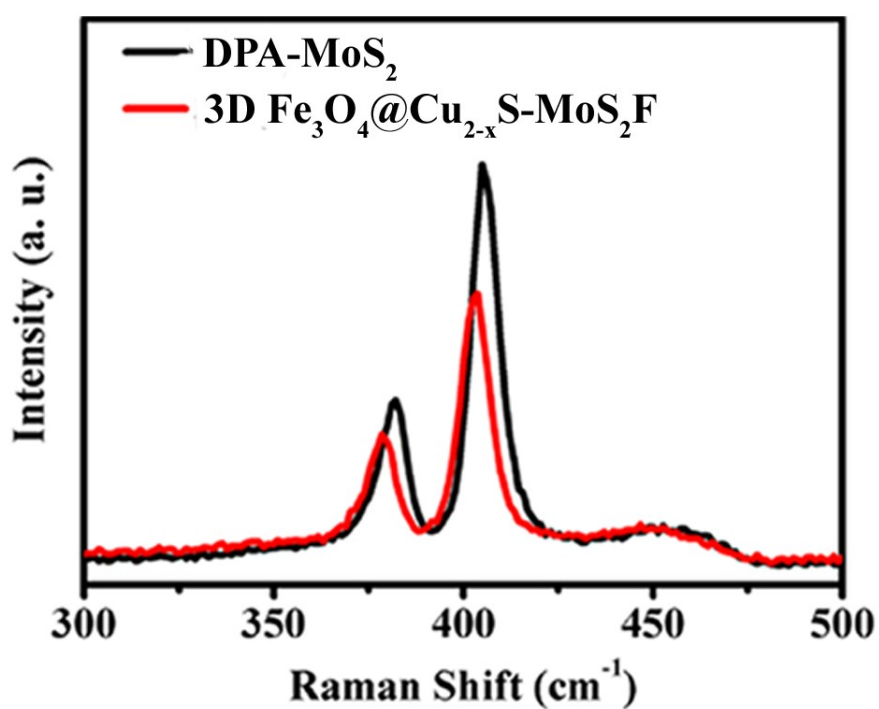


Figure S4. Raman spectra of the 3D $\text{Fe}_3\text{O}_4@Cu_{2-x}\text{S-MoS}_2\text{F}$ and DPA- MoS_2 .

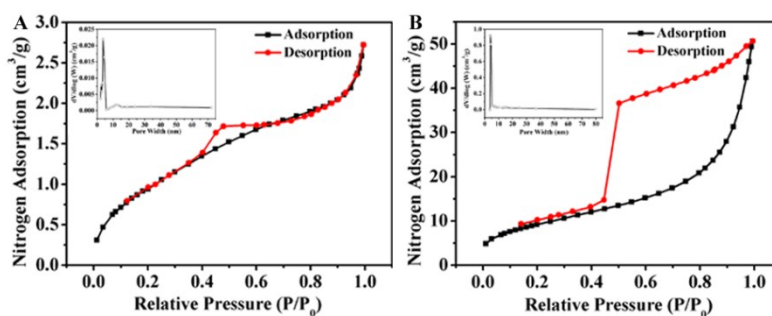


Figure S5. Nitrogen adsorption/desorption isotherms of the $\text{Fe}_3\text{O}_4@\text{Cu}_{2-x}\text{S}$ NPs (A) and physical mixing of $\text{Fe}_3\text{O}_4@\text{Cu}_{2-x}\text{S}$ NPs and MoS_2 NSs (B). Inset: the pore size distribution of the $\text{Fe}_3\text{O}_4@\text{Cu}_{2-x}\text{S}$ NPs (A inset) and physical mixing of $\text{Fe}_3\text{O}_4@\text{Cu}_{2-x}\text{S}$ NPs and MoS_2 NSs (B inset).

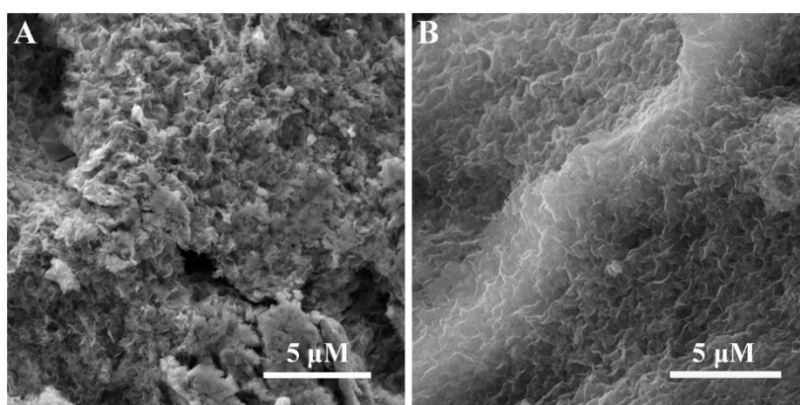


Figure S6. SEM images of physical mixing of $\text{Fe}_3\text{O}_4@\text{Cu}_{2-x}\text{S}$ NPs and MoS_2 NSs (A) and 3D $\text{Fe}_3\text{O}_4@\text{Cu}_{2-x}\text{S}-\text{MoS}_2\text{F}$ (B).

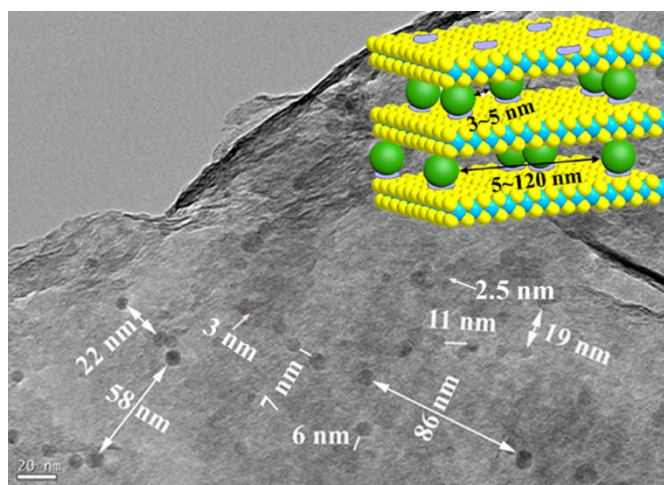


Figure S7. TEM image of 3D $\text{Fe}_3\text{O}_4@\text{Cu}_{2-x}\text{S}-\text{MoS}_2\text{F}$. The inset shows the simulation diagram of the formed 3D $\text{Fe}_3\text{O}_4@\text{Cu}_{2-x}\text{S}-\text{MoS}_2\text{F}$. There are two types pores in Figure 3B. In order to explore the reasons, we have complemented the N_2 adsorption and pore size distribution of pure $\text{Fe}_3\text{O}_4@\text{Cu}_{2-x}\text{S}$ NPs and physical mixing of $\text{Fe}_3\text{O}_4@\text{Cu}_{2-x}\text{S}$ NPs and MoS_2 NSs (**Figure S5**). Brunauer Emmett Teller (BET) analysis shown that the specific surface areas of $\text{Fe}_3\text{O}_4@\text{Cu}_{2-x}\text{S}$ NPs and physical mixing of $\text{Fe}_3\text{O}_4@\text{Cu}_{2-x}\text{S}$ NPs and MoS_2 NSs are $3.838 \text{ m}^2 \text{ g}^{-1}$ and $33.719 \text{ m}^2 \text{ g}^{-1}$ respectively, which is smaller than the 3D $\text{Fe}_3\text{O}_4@\text{Cu}_{2-x}\text{S}-\text{MoS}_2\text{F}$ ($66.85 \text{ m}^2 \text{ g}^{-1}$). The pore-size

distributions of the pure $\text{Fe}_3\text{O}_4@\text{Cu}_{2-x}\text{S}$ NPs and mixing of two units are in the range of 1.94-5.7 nm and 3.69-5.22 nm, respectively. In addition, combined with the different morphology of the physical mixing of $\text{Fe}_3\text{O}_4@\text{Cu}_{2-x}\text{S}$ NPs and MoS_2 NSs and 3D $\text{Fe}_3\text{O}_4@\text{Cu}_{2-x}\text{S}-\text{MoS}_2\text{F}$ (**Figure S6**), we conclude that 3D $\text{Fe}_3\text{O}_4@\text{Cu}_{2-x}\text{S}-\text{MoS}_2\text{F}$ and the physical mixing sample have different structures. All of the above results indicated that the formation of 3D porous $\text{Fe}_3\text{O}_4@\text{Cu}_{2-x}\text{S}-\text{MoS}_2\text{F}$ is not a simple physical mixing of MoS_2 nanosheets and $\text{Fe}_3\text{O}_4@\text{Cu}_{2-x}\text{S}$ NPs.

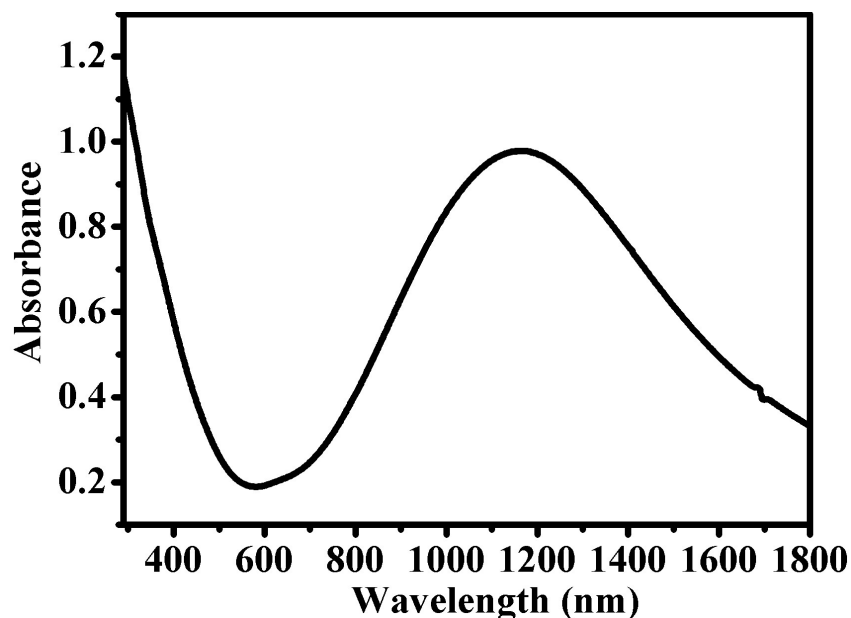


Figure S8 Corresponding UV-vis-NIR absorption spectra of the $\text{Fe}_3\text{O}_4@\text{Cu}_{2-x}\text{S}$ nanoparticles dispersed in chloroform.

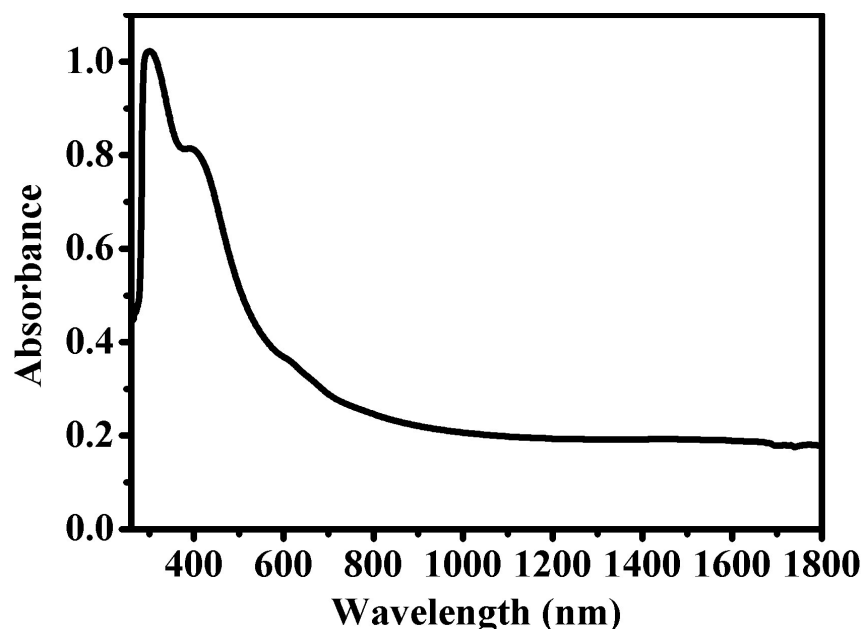


Figure S9. UV-vis-NIR absorption spectra of the MoS_2 dispersed in DMF.

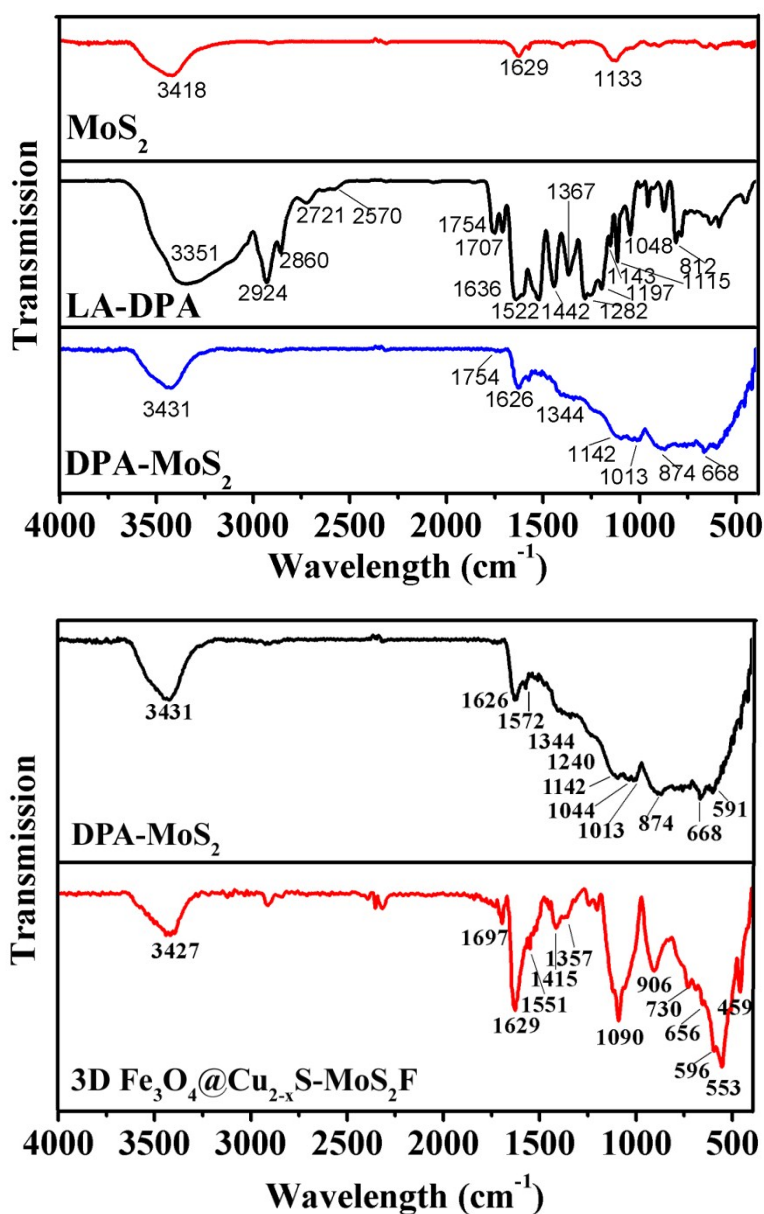


Figure S10. IR spectra of MoS₂, LA-DPA, DPA-MoS₂ and 3D Fe₃O₄@Cu_{2-x}S-MoS₂F. As shown in Figure S10, the FT-IR spectra of LA-DPA revealed the exposed S-S band at 2570 cm⁻¹. This peak becomes absent after conjugation with MoS₂ NSs, indicating that the S-S moiety becomes buried on to the MoS₂ surface.⁶ Due to coordination between the phenolic hydroxyl group of DPA-MoS₂ and Fe₃O₄@Cu_{2-x}S NPs,⁷ a new absorption peak at 1090 cm⁻¹ corresponding to C-O-Cu vibration was observed in the formed 3D Fe₃O₄@Cu_{2-x}S-MoS₂F, while the peak of the phenolic $\nu_{(C-O)}$ at 1142 cm⁻¹ appeared in DPA-MoS₂ was disappeared. Moreover, the Fe-O and Cu-O absorption bands are appeared at 596, 553 and 459 cm⁻¹.⁸

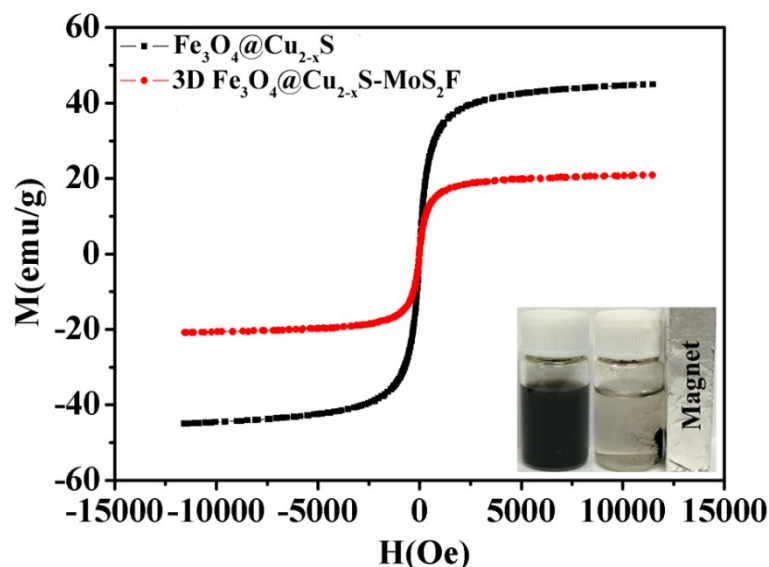


Figure S11. Magnetization hysteresis loops of $\text{Fe}_3\text{O}_4@\text{Cu}_{2-x}\text{S}$ NPs and the $3\text{D Fe}_3\text{O}_4@\text{Cu}_{2-x}\text{S-MoS}_2\text{F}$ at room temperature. The $3\text{D Fe}_3\text{O}_4@\text{Cu}_{2-x}\text{S-MoS}_2\text{F}$ showed no remanence magnetization or coercivity at 300 K, indicating that the superparamagnetic property makes the hybrids suitable for controlled magnetic manipulation. It's worth noting that the saturated mass magnetization of the $3\text{D Fe}_3\text{O}_4@\text{Cu}_{2-x}\text{S-MoS}_2\text{F}$ is 20.82 emu/g, which is lower than that of $\text{Fe}_3\text{O}_4@\text{Cu}_{2-x}\text{S}$ nanoparticle control (44.96 emu/g). The decreased saturated mass magnetization is due to the nonmagnetic MoS_2 materials.

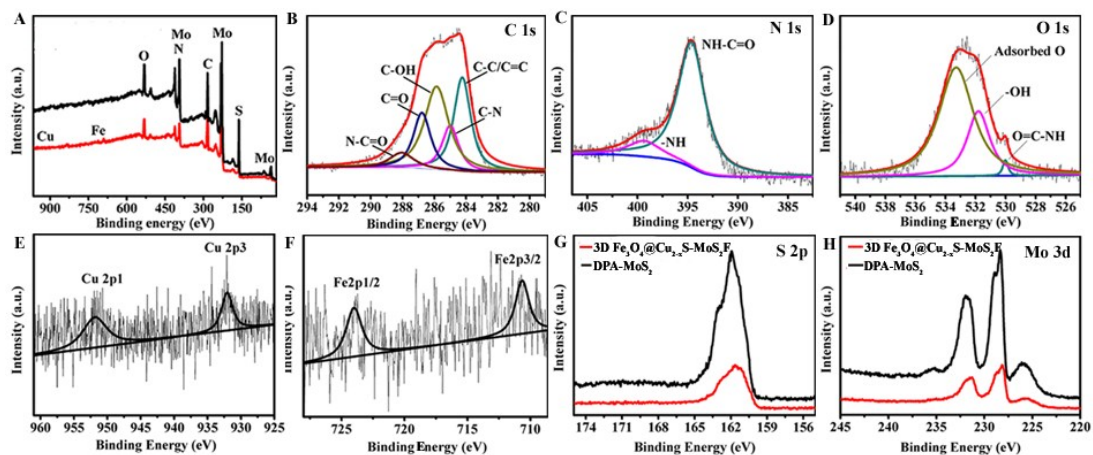


Figure S12. (A) XPS survey spectrum of the $3\text{D Fe}_3\text{O}_4@\text{Cu}_{2-x}\text{S-MoS}_2\text{F}$ (red line) and DPA-MoS_2 (black line). High-resolution scans for the C 1s (B), N 1s (C), O 1s (D), Cu 2p (E) and Fe 2p (F) electrons of the $3\text{D Fe}_3\text{O}_4@\text{Cu}_{2-x}\text{S-MoS}_2\text{F}$. High-resolution scans for the S 2p (G) and Mo 3d (H) electrons.

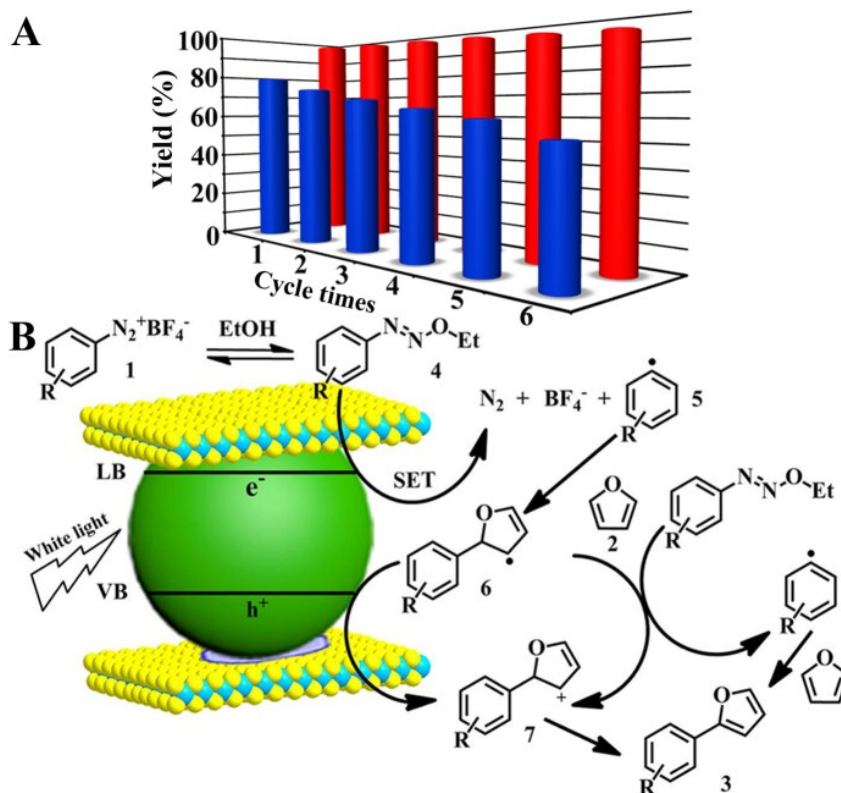


Figure S13. (A) Catalytic cycle of the Fe₃O₄@Cu_{2-x}S nanoparticles (blue column) and the 3D Fe₃O₄@Cu_{2-x}S-MoS₂F (red column). (B) Postulated reaction mechanism for the 3D Fe₃O₄@Cu_{2-x}S-MoS₂F-mediated direct arylation of heteroarenes.

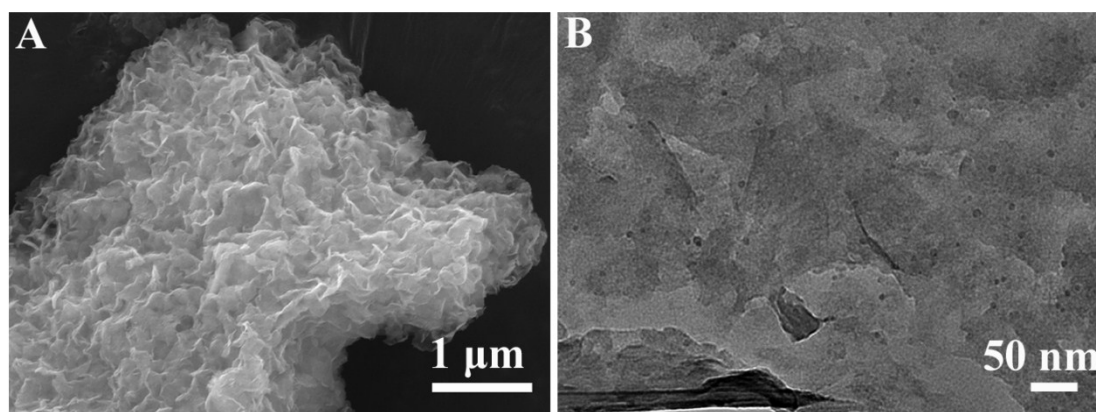


Figure S14. SEM (A) and TEM (B) images of the 3D Fe₃O₄@Cu_{2-x}S-MoS₂F after reusing 6 times.

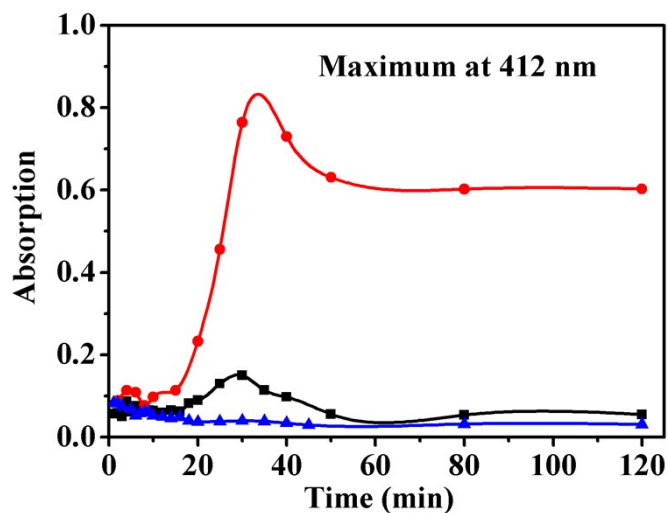


Figure S15. Reaction kinetic of formation and decomposition of azoether **4a** (R = 4-Cl) via detection of absorption maximum at 412 nm. Blue line : Standard reaction. Black line : Reaction without Furan. Red line : Reaction without 3D Fe₃O₄@Cu_{2-x}S-MoS₂F. In order to investigate the plausible mechanism for this photoreaction, the standard reactions with diazo compound **1a** (R = 4-Cl) were carried out. In the standard reaction without 3D Fe₃O₄@Cu_{2-x}S-MoS₂F, an absorption maximum at 412 nm could be detected after ten minutes and the intensity reached to maximum quickly. However the intensity decreased slowly and was still existence after 120 minutes. When the reaction was conducted without furan, no obvious maximum was observed over a period of 120 minutes. These results indicated that the diazonium salt reacts with the alcohol to form an intermediate which was assigned to the azoether **4a**. In addition, furan acted as a weak base in the reaction could help the formation of the azoether. Interestingly, there was no absorption maximum over a period of 2 h. in the standard reaction. This phenomenon could be due to the excellent catalytic performance of 3D Fe₃O₄@Cu_{2-x}S-MoS₂F. In other words, the 3D Fe₃O₄@Cu_{2-x}S-MoS₂F could catalyze the conversion of azoether **4a** to aryl radical **5a** as soon as the azoether generated in the presence of furan. Therefore, the conversion rate is too fast to detect the azoether.

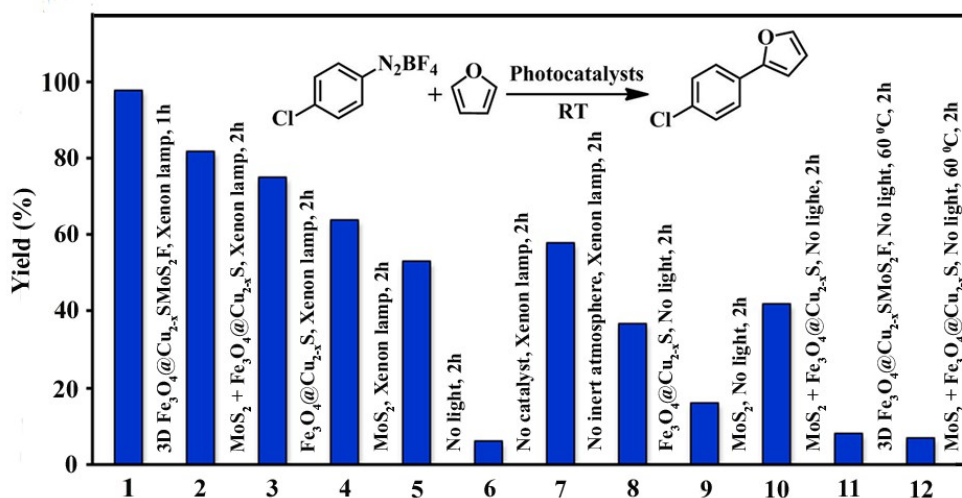
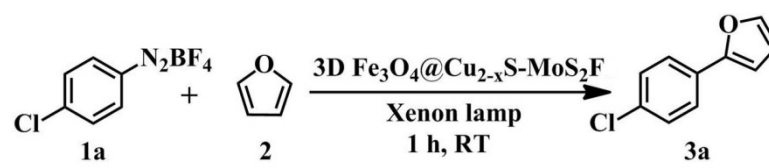


Figure S16. Conversion comparison with different catalysts under various catalytic conditions.

Table S1. Optimization of Reaction Conditions.


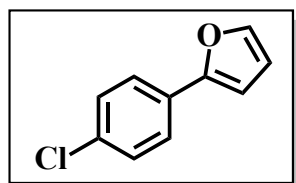
entry	reaction conditions	yield [%]
1	DMSO/2 (1:1)	48%
2	DMF/2 (1:1)	30%
3	MeCN/2 (1:1)	19%
4	Aceton/2 (1:1)	41%
5	MeOH/2 (1:1)	93%
6	EtOH/2 (1:1)	98%
7	Isopropanol/2 (1:1)	47%
8	1,4-dioxane /2 (1:1)	34%

Reaction conditions: 0.1 mmol **1a**, 2 mg 3D Fe₃O₄@Cu_{2-x}S-MoS₂F, 1 mL solvent, 1 mL furan, irradiation with Xenon lamp equipped with 700nm cutoff filter for 1 h under argon atmosphere. All the yields were determined by GC.

Among the different solvents tested (Table S1), ethanol was found to be a good solvent for the photoreaction (Table S1 entry 6). Meanwhile, the photocatalytic activities of MoS₂, Fe₃O₄@Cu_{2-x}S, simply mixed Fe₃O₄@Cu_{2-x}S and MoS₂, and Fe₃O₄@Cu_{2-x}S-MoS₂F without light were also carried out. As shown in Figure S16, the use of Fe₃O₄@Cu_{2-x}S-MoS₂F catalyst resulted in > 98% yield under NIR light. However, no traceable products were detected for control experiments. Also, we found that the photocatalytic activity of the Fe₃O₄@Cu_{2-x}S sample and simply mixed Fe₃O₄@Cu_{2-x}S and MoS₂ was significantly lower than that of the Fe₃O₄@Cu_{2-x}S-MoS₂F sample, which reveals that the 3D porous assembly structure plays an important role for the enhancement of the photocatalytic activity.

Characterization of synthesized products:

2-(4-Chlorophenyl)furan⁹



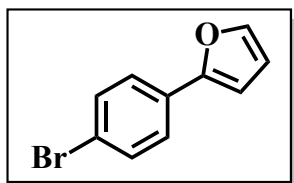
¹H-NMR (400 MHz, CDCl₃):

δ /ppm = 7.569-7.591 (d, J = 8.8 Hz, 2H), 7.45-7.457 (dd, J = 1.6 Hz, J = 0.8 Hz, 1H), 7.323-7.345 (d, J = 8.8 Hz, 2H), 6.619-6.629 (dd, J = 3.2 Hz, J = 0.8 Hz, 1H), 6.454-6.467 (dd, J = 3.6 Hz, J = 1.6 Hz, 1H).

¹³C-NMR (100 MHz, CDCl₃):

δ /ppm = 153.0, 142.4, 133.0, 129.4, 129.0, 125.1, 111.9, 105.5.

2-(4-Bromophenyl)furan⁹



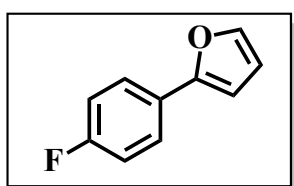
¹H-NMR (400 MHz, CDCl₃):

δ /ppm = 7.482-7.543 (m, 4H), 7.466-7.469 (dd, $J = 1.8$ Hz, $J = 0.6$ Hz, 1H), 6.653-6.644 (dd, $J = 3.4$ Hz, $J = 0.6$ Hz, 1H), 6.464-6.477 (dd, $J = 3.2$ Hz, $J = 2.0$ Hz, 1H).

¹³C-NMR (100 MHz, CDCl₃):

δ /ppm = 153.0, 142.5, 131.9, 129.8, 125.4, 121.1, 111.9, 105.6.

2-(4-Fluorophenyl)furan¹⁰



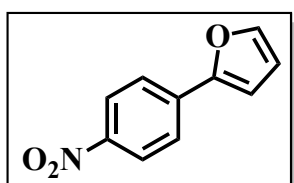
¹H-NMR (400 MHz, CDCl₃):

δ /ppm = 7.598-7.635 (m, 2H), 7.430-7.434 (dd, $J = 1.8$ Hz, $J = 0.6$ Hz, 1H), 7.034-7.078 (m, 2H), 6.556-6.564 (d, $J = 3.2$ Hz, 1H), 6.437-6.449 (dd, $J = 3.2$ Hz, $J = 1.6$ Hz, 1H).

¹³C-NMR (100 MHz, CDCl₃):

δ /ppm = 163.4, 161.0, 153.2, 142.1, 127.4 (d, $J = 2.8$ Hz), 125.6 (d, $J = 8.6$ Hz), 115.7 (d, $J = 21.9$ Hz), 111.8, 104.7.

2-(4-Nitrophenyl)furan⁹



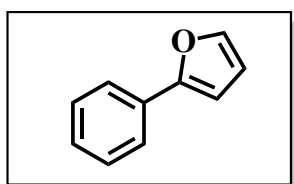
¹H-NMR (400 MHz, CDCl₃):

δ /ppm = 8.218-8.238 (d, $J = 8.0$ Hz, 2H), 7.76-7.781 (d, $J = 8.4$ Hz, 2H), 7.567 (d, $J = 1.8$ Hz, 1H), 6.870-6.878 (dd, $J = 3.6$ Hz, $J = 0.5$ Hz, 1H), 6.545-6.554 (dd, $J = 3.6$ Hz, $J = 1.6$ Hz, 1H).

¹³C-NMR (100 MHz, CDCl₃):

δ /ppm = 151.7, 146.4, 144.2, 136.5, 124.4, 124.0, 112.5, 109.1.

2-Phenylfuran⁹



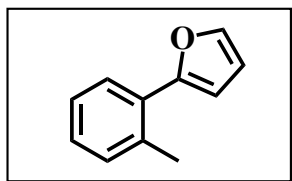
¹H-NMR (400 MHz, CDCl₃):

δ /ppm = 7.659-7.682 (m, 2H), 7.449,7.451,7.454,7.456 (dd, $J = 2.0$ Hz, $J = 0.8$ Hz, 1H), 7.349-7.388 (m, 2H), 7.243-7.261 (m, 1H), 6.634-6.642 (dd, $J = 3.2$ Hz, $J = 0.7$ Hz, 1H), 6.448-6.461 (dd, $J = 3.2$ Hz, $J = 2.0$ Hz, 1H).

^{13}C -NMR (100 MHz, CDCl_3):

δ /ppm = 154.1, 142.2, 131.0, 128.8, 127.5, 123.9, 111.8, 105.1.

2-(2-Methylphenyl) furan¹¹



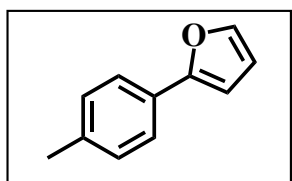
^1H -NMR (400 MHz, CDCl_3):

δ /ppm = 7.684-7.703 (dd, $J = 7.6$ Hz, $J = 2.0$ Hz, 1H), 7.497-7.502 (dd, $J = 2.0$ Hz, $J = 0.8$ Hz, 1H), 7.198-7.246 (m, 3H), 6.532-6.538 (dd, $J = 3.4$ Hz, $J = 0.7$ Hz, 1H), 6.488-6.501 (dd, $J = 3.2$ Hz, $J = 2.0$ Hz, 1H), 1.84, 2.8, 1H), 2.491 (s, 3H).

^{13}C -NMR (100 MHz, CDCl_3):

δ /ppm = 153.6, 141.8, 134.7, 131.2, 130.3, 127.6, 127.1, 126.1, 111.4, 108.6, 22.0.

2-(4-Methylphenyl) furan⁹



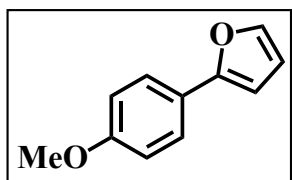
^1H -NMR (400 MHz, CDCl_3):

δ /ppm = 7.544-7.565 (d, $J = 8.4$ Hz, 2H), 7.414-7.419 (d, $J = 1.8$ Hz, 1H), 7.156-7.175 (d, $J = 7.6$ Hz, 2H), 6.563-6.573 (d, $J = 3.2$ Hz, 1H), 6.422-6.434 (dd, $J = 3.2$ Hz, $J = 1.6$ Hz, 1H), 2.332 (s, 3H).

^{13}C -NMR (100 MHz, CDCl_3):

δ /ppm = 154.3, 141.8, 137.3, 129.5, 128.4, 123.9, 111.7, 104.4, 21.4.

2-(4-Methoxyphenyl)furan⁹



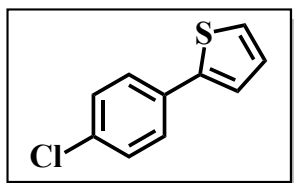
^1H -NMR (400 MHz, CDCl_3):

δ /ppm = 7.577-7.60 (d, $J = 9.2$ Hz, 2H), 7.404-7.409 (dd, $J = 1.8$ Hz, $J = 0.8$ Hz, 1H), 6.888-6.911 (d, $J = 9.2$ Hz, 2H), 6.491-6.500 (dd, $J = 3.6$ Hz, $J = 0.6$ Hz, 1H), 6.419-6.432 (dd, $J = 3.2$ Hz, $J = 2.0$ Hz, 1H), 3.79 (s, 3H).

^{13}C -NMR (100 MHz, CDCl_3):

δ /ppm = 159.1, 154.1, 141.5, 125.3, 124.1, 114.2, 111.7, 103.5, 55.4.

2-(4-Chlorophenyl)thiophene¹²



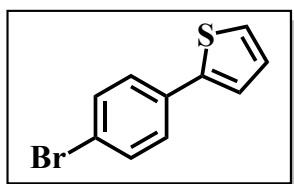
¹H-NMR (400 MHz, CDCl₃):

δ /ppm = 7.50-7.52 (m, 2H), 7.31-7.38 (m, 2H), 7.24-7.27 (m, 2H), 7.04-7.07 (m, 1H); **¹³C-NMR**

(100 MHz, CDCl₃):

δ /ppm = 143.2, 133.2, 133.0, 129.1, 128.2, 127.1, 125.3, 123.4.

2-(4-Bromophenyl)thiophene¹³



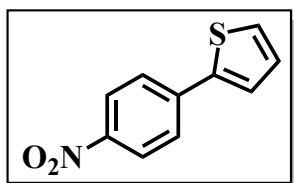
¹H-NMR (400 MHz, CDCl₃):

δ /ppm = 7.38-7.47 (m, 4H), 7.28-7.30 (d, $J = 4.3$ Hz, 2H), 7.03-7.05 (m, 1H).

¹³C-NMR (100 MHz, CDCl₃):

δ /ppm = 143.2, 133.4, 132.1, 128.3, 127.5, 125.4, 123.6, 121.4.

2-(4-Nitrophenyl)thiophene¹⁴



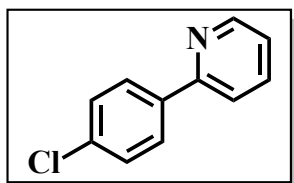
¹H-NMR (400 MHz, CDCl₃):

δ /ppm = 8.222-8.245 (m, 2H), 7.727-7.750 (m, 2H), 7.473-7.485 (dd, $J = 3.6$ Hz, $J = 1.2$ Hz, 1H),
7.435-7.450 (dd, $J = 5.2$ Hz, $J = 1.2$ Hz, 1H), 7.142-7.165 (dd, $J = 5.2$ Hz, $J = 3.6$ Hz, 1H).

¹³C-NMR (100 MHz, CDCl₃):

δ /ppm = δ 146.6, 141.7, 140.7, 128.8, 127.8, 126.1, 125.8, 124.5.

2-(4-Chlorophenyl)pyridine¹⁵



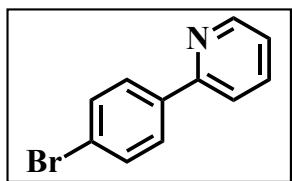
¹H-NMR (400 MHz, CDCl₃):

δ /ppm = 8.681-8.694 (d, $J = 4.8$ Hz, 1H), 7.927-7.949 (d, $J = 8.8$ Hz, 2H), 7.738-7.781 (td, $J = 1.8$ Hz, $J = 1.8$ Hz, 1H), 7.687-7.707 (d, $J = 8.0$ Hz, 1H), 7.434-7.456 (d, $J = 8.8$ Hz, 2H), 7.233-7.265 (m, 1H).

¹³C-NMR (100 MHz, CDCl₃):

δ/ppm = 156.3, 149.8, 137.8, 137.0, 135.2, 129.0, 128.3, 122.5, 120.5.

2-(4-Bromophenyl) pyridine¹⁶



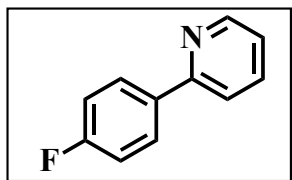
¹H-NMR (400 MHz, CDCl₃):

δ/ppm = 8.655-8.671 (ddd, $J = 4.8$ Hz, $J = 1.8$ Hz, $J = 1.0$ Hz, 1H), 7.834-7.868 (m, 2H), 7.708-7.731 (m, 1H), 7.661-7.684 (dt, $J = 8.0$ Hz, $J = 1.2$ Hz, 1H), 7.567-7.595 (m, 2H), 7.211-7.246 (m, 1H).

¹³C-NMR (100 MHz, CDCl₃):

δ/ppm = 156.3, 149.9, 137.0, 132.0, 128.6, 123.5, 122.6, 120.4.

2-(4-Fluorophenyl) pyridine¹⁷



¹H-NMR (400 MHz, CDCl₃):

δ/ppm = 8.673 (m, 1H), 7.957-7.992 (m, 2H), 7.667-7.765 (m, 2H), 7.135-7.264 (m, 3H).

¹³C-NMR (100 MHz, CDCl₃):

δ/ppm = 164.8, 162.3, 156.5, 149.8, 137.0, 135.6 (d, $J = 2.7$ Hz), 128.8 (d, $J = 7.7$ Hz), 122.2, 120.4, 115.7 (d, $J = 21.9$ Hz).

REFERENCES

- 1 (a) S. S. Chou, M. De, J. Kim, S. Byun, C. Dykstra, J. Yu, J. X. Huang and V. P. Dravid, *J. Am. Chem. Soc.*, 2013, **135**, 4584-4587. (b) T. Liu, C. Wang, W. Cui, H. Gong, C. Liang, X. Z. Shi, Z. W. Li, B. Q. Sun and Z. Liu, *Nanoscale*, 2014, **6**, 11219-11225.
- 2 Q. W. Tian, J. Q. Hu, Y. H. Zhu, R. J. Zou, Z. G. Chen, S. P. Yang, R. W. Li, Q. Q. Su, Y. Han and X. G. Liu, *J. Am. Chem. Soc.*, 2013, **135**, 8571-8577.
- 3 B. D. Wang, B. G. Wang, P. F. Wei, X. B. Wang and W. J. Lou, *Dalton Trans.*, 2012, **41**, 896-899.
- 4 L. Y. Wang, G. W. Hu, Z. Y. Wang, B. D. Wang, Y. M. Song and H. A. Tang, *RSC Adv.*, 2015, **5**, 73327-73332.
- 5 P. Hanson, J. R. Jones, A. B. Taylor, P. H. Walton and A. W. Timms, *J. Chem. Soc., Perkin Trans.*, 2002, **2**, 1135-1150.

- 6 (a) S. S. Chou, M. De, J. Kim, S. Byun, C. Dykstra, J. Yu, J. X. Huang and V. P. Dravid, *J. Am. Chem. Soc.*, 2013, **135**, 4584-4587. (b) W. Shi, Y. Sahoo, M. T. Swihart, *Colloids and Surfaces A: Physicochem. Eng. Aspects*, 2004, **246**, 109-113. (c) P. Thangadurai, S. Balaji, P. T. Manoharan, *Nanotechnology*, **2008**, 19, 435708.
- 7 T. Fujii, F. M. F. Groot, G. A. Sawatzky, F. C. Voogt, T. Hibma and K. Okada, *Phys. Rev. B.*, 1999, **59**, 3195-3202.
- 8 J. Liu, Z. K. Sun, Y. H. Deng, Y. Zou, C. Y. Li, X. H. Guo, L. Q. Xiong, Y. Gao, F. Y. Li and D. Y. Zhao, *Angew. Chem., Int. Ed.*, 2009, **121**, 5989-5993.
- 9 C.-Y. Zhou, P. W. H. Chan and C.-M. Che, *Org. Lett.*, 2006, **8**, 325-328.
- 10 S. K. Guchhait, M. Kashyap and S. Saraf, *Synthesis*, 2010, 1166-1170.
- 11 S. E. Denmark, J. D. Baird and C. S. Regens, *J. Org. Chem.*, 2008, **73**, 1440-1455.
- 12 N. Kuhl, M. N. Hopkinson and F. Glorius, *Angew. Chem. Int. Ed.*, 2012, **51**, 8230-8234.
- 13 N. Uchiyama, E. Shirakawa, R. Nishikawa and T. Hayashi, *Chem. Commun.*, 2011, **47**, 11671-11673.
- 14 J. H. Li, Y. Liang, D. P. Wang, W. J. Liu, Y. X. Xie and D. L. Yin, *J. Org. Chem.*, 2005, **70**, 2832-2834.
- 15 Y. Kitamura, S. Sako, T. Udzu, A. Tsutsui, T. Maegawa, Y. Monguchi and H. Sajiki, *Chem. Commun.*, 2007, 5069-5071.
- 16 J. Sun, W. Wu and J. Zhao, *Chem. Eur. J.*, 2012, **18**, 8100-8112.
- 17 L. Ackermann, H. K. Potukuchi, A. R. Kapdi and C. Schulzke, *Chem. Eur. J.*, 2010, **16**, 3300-3303.